Interchange Instability and Transport in Matter-Antimatter Plasmas

Alexander Kendl,* Gregor Danler, Matthias Wiesenberger, and Markus Held
Institut für Ionenphysik und Angewandte Physik, Universität Innsbruck, Technikerstrasse 25, 6020 Innsbruck, Austria
(Received 25 November 2016; revised manuscript received 17 March 2017; published 6 June 2017)

Symmetric electron-positron plasmas in inhomogeneous magnetic fields are intrinsically subject to interchange instability and transport. Scaling relations for the propagation velocity of density perturbations relevant to transport in isothermal magnetically confined electron-positron plasmas are deduced, including damping effects when Debye lengths are large compared to Larmor radii. The relations are verified by nonlinear full-F gyrofluid computations. Results are analyzed with respect to planned magnetically confined electron-positron plasma experiments. The model is generalized to other matter-antimatter plasmas. Magnetized electron-positron-proton-antiproton plasmas are susceptible to interchange-driven local matter-antimatter separation, which can impede sustained laboratory magnetic confinement.

DOI: 10.1103/PhysRevLett.118.235001

Antimatter, predicted by Dirac less than a century ago [1], has so far made its earthly appearance through cosmic and laboratory high-energy events only in exiguous quantities [2] or rather brief periods [3] before annihilating again. Macroscopic amounts of mixed matter-antimatter in the form of relativistic electron-positron pair plasmas are presumed to exist at the highest energy density astrophysical objects, such as active galactic nuclei, pulsars, and black holes [4]. The extended confinement of larger numbers than a few antimatter particles in the laboratory is impeded by instant annihilation at contact with materials. Ion and atom traps have been used to confine clouds of positrons or antihydrogen [5,6]. The investigation of many-body antimatter physics on long time scales and low densities should be feasible in magnetically confined quasineutral systems of charged particles [7–9]. For short times, high-density matter-antimatter plasmas could be achieved by laser-target interaction [3].

The most basic matter-antimatter system conceivable in the laboratory is a classical plasma with equal amounts of electrons and positrons. An electron-positron (e-p) pair plasma is a unique many-body system and distinct from a classical electron-ion (e-i) plasma in its intrinsic mass symmetry. Many fundamental instabilities that are abundant in mass-asymmetric e-i plasmas are absent in e-p systems [7]. Microinstabilities like drift waves in magnetized e-i plasmas generically result in turbulent transport losses across the confining magnetic field [10]. The absence or weakness of instabilities and turbulence is consequently crucial for the quality of planned magnetically confined e-p plasma experiments [8]. Classical resistive drift wave instabilities, which rely on asymmetry in the motion of electrons and ions parallel to the magnetic field $\mathbf{B}$ with mass ratio $m_e/m_i \ll 1$, are nonexistent in e-p plasmas. Magnetic curvature-induced drift-interchange modes driven by a temperature gradient have been shown to be suppressed for low e-p plasma densities by an effective screening of electric potential fluctuations on scales smaller than the Debye length [8,11,12].

Cross-field pressure-driven interchange motion and instability of plasma perturbations is achievable not only in the presence of temperature gradients, but also for isothermal plasmas in the presence of a density gradient. Local field-aligned (flutelike) density perturbations with a positive amplitude, sometimes termed "blobs," can be pushed across the magnetic field (down the field gradient) by their own intrinsic density inhomogeneity [13,14]. This instability mechanism is similar (and in reduced models isomorphic) to the buoyancy-driven convection of fluids with a pressure gradient [15]: While the familiar Rayleigh-Bénard convective motion feeds on the gravitational potential energy, the magnetized plasma interchange instability is driven by the energy stored in the inhomogeneity of the confining magnetic equilibrium field, which acts like an effective gravity. Both mechanisms generate vorticity that leads to propagating plume structures. In magnetized plasmas, the fluidlike motion perpendicular to the magnetic field is governed by drifts, which describe the mean motion on top of the fast gyration of the charged particles. In the case at hand, curvature and magnetic gradient drifts at pressure gradients perpendicular to the equilibrium profiles and magnetic field are responsible for the separation of differently charged species, and for polarization drifts, which respond to maintain quasineutrality. A dipolar electric potential is formed which transports the perturbation down the magnetic field gradient by $\mathbf{E} \times \mathbf{B}$ drift convection [15].

Here we show that density blobs in an inhomogeneously magnetized e-p plasma are interchange unstable for a range of accessible parameters and can lead to crucial transport losses. We further consider more general matter-antimatter plasmas consisting of initially equal electron, proton, positron, and antiproton densities (which could in some future experiment be feasible but is cosmologically probably irrelevant) and show that the interchange instability leads not only to transport but also to matter-antimatter separation.

First, we analyze magnetized e-p plasmas by means of a full-F gyrofluid model [16], which is derived from a gyrokinetic model that evolves the full distribution function $F(\mathbf{x}, \mathbf{v}, t)$. In the isothermal 2D limit [17,18] the model consists of continuity equations for the gyrocenter densities n_s for electron and positron species $s \in (e, p)$:

$$\partial_t n_s = [n_s, \psi_s] + n_s \hat{\kappa}(\psi_s) + \tau_s \hat{\kappa}(n_s), \tag{1}$$

coupled to the electric potential ϕ in Poisson's equation:

$$\sum_s Z_s N_s + \varepsilon \nabla_\perp^2 \phi = 0. \tag{2}$$

Exact local quasineutrality is thus violated for $\varepsilon \neq 0$. The particle densities N_s with charge states $Z_e = -1$ and $Z_p = +1$ are linked to the gyrocenter densities n_s via

$$N_s = \Gamma_{1s} n_s + \boldsymbol{\nabla} \cdot (n_s \mu_s Z_s^{-1} \boldsymbol{\nabla}_\perp \phi). \tag{3}$$

The divergence term in Eq. (3) implicitly covers the effects of polarization drifts (which explicitly appear in fluid but not gyrofluid models). In contrast to quasineutral e-i systems as in Ref. [16], we retain the Debye parameter $\varepsilon = (\lambda/\rho)^2$, which represents the effects of finite Debye length $\lambda = \sqrt{\epsilon_0 T_e/(e^2 N_{e0})}$ in relation to the Larmor radius $\rho = \sqrt{T_e m_e}/(eB)$. Here T_e and m_e are the electron temperature and mass, respectively. The temperature ratio is $\tau_s = T_s/(Z_s T_e)$, so that $\tau_e = -1$ and $\tau_p \geq 0$. The e-p mass ratios $\mu_s = m_s/m_p = 1$ are both unity, so that $\mu \equiv \sum_s \mu_s = 2$. Annihilation between positrons and electrons is here neglected for the time scales of radial transport [19].

Finite Larmor radius (FLR) and ponderomotive effects enter via $\psi_s = \Gamma_{1s}\phi - (1/2)(\mu_s/Z_s)(\nabla_\perp \phi)^2$ for constant B. The gyroaveraging operator is given by $\Gamma_{1s} = [1 + (1/2)b_s]^{-1}$ with $b_s = -(\mu_s \tau_s / Z_s)\nabla_\perp^2$. The gyrocenter densities are normalized to a reference density n_0, the potential to T_e/e, length scales to ρ, and time to c_s/ρ with sound speed $c_s = \sqrt{T_e/m_e}$. The 2D advection terms are expressed through Poisson brackets $[f, g] = (\partial_x f)(\partial_y g) - (\partial_y f)(\partial_x g)$ for local coordinates x and y perpendicular to $\mathbf{B}$. Normal magnetic curvature $\kappa = \partial_x \ln B \equiv 2\rho/R$ enters into $\hat{\kappa} = \kappa \partial_y$. For toroidal confinement $\rho \ll R$, the torus radius, so that $\kappa \ll 1$.

We analyze the dependence of the interchange growth rate on the Debye screening parameter ε by linearizing Eqs. (1) and (2) on top of a background density $n_0(\mathbf{x})$ for small perturbation amplitudes $\tilde{n}_e, \tilde{n}_p, \tilde{\phi} \sim \exp(-i\omega t + i\mathbf{k} \cdot \mathbf{x})$. Neglecting FLR effects ($b_s \equiv 0$), we get

$$-\omega \tilde{n}_s = (\omega_c - \omega_*)\tilde{\phi} + \tau_s \omega_c \tilde{n}_s, \tag{4}$$

$$(\mu + \varepsilon) k_\perp^2 \tilde{\phi} = \tilde{n}_p - \tilde{n}_e. \tag{5}$$

Here $\omega_c = \kappa k_y$ and $\omega_* = -g k_y$, with $g = \partial_x \ln n = g_0 + g_1$ composed of a background density gradient g_0 and a contribution g_1 by the intrinsic perturbation front. For $\omega = \omega_r + i\gamma$, we obtain a growth rate γ with

$$\gamma^2 = \frac{1+\tau}{\mu+\epsilon}\left[\frac{\omega_c}{k_\perp^2}(\omega_* - \omega_c) - \frac{1}{4}(\mu+\epsilon)(1+\tau)\omega_c^2\right]. \tag{6}$$

The model is unstable for $\gamma^2 > 0$. For e-p plasmas $\mu = 2$ (with $\tau \equiv \tau_p$ and $\tau_e = -1$), whereas for quasineutral e-i plasmas we would have $\mu = 1$ and $\epsilon = 0$.

We apply the blob correspondence principle [13] by assuming that the mode most relevant for instability of the blob front is of the blob scale σ. This situation is illustrated on the left in Fig. 1: Initially circular perturbations with a density maximum in the center have an intrinsic pressure gradient pointing from all sides to the maximum. Instability is [for $k_\perp^2 \ll 1$ in Eq. (6)] achieved when $\omega_c < \omega_*$ and thus $\kappa < -g = -\partial_x \ln \tilde{n}$. This can be fulfilled only on the right half circle of the perturbation (shaded area), and the growth is maximum at the strongest gradient (orange area), which is shifted to the right in the shape of a propagating plume.

For Gaussian blobs with width σ, this relates to $k_y = k_x \approx 1/\sigma$ and $k_\perp^2 \approx 2/\sigma^2$. Relating the growth rate to blob convection, the propagation velocity is approximated as $v_x = \sigma\gamma$. We here neglect a background gradient, so that $g = g_1 \approx (1/n_0)\partial_x n$ is evaluated for an initial blob density $n(\mathbf{x}) = n_0 + A\exp(-\mathbf{x}^2/\sigma^2)$ at $x = \sigma/\sqrt{2}$ to be $g_1 = -a/\sigma$ with $a \approx 0.86A$. We obtain

$$v_x = \frac{1}{\sqrt{1+(\varepsilon/2)}}\sqrt{\frac{1}{2}a\kappa\sigma - \kappa^2\sigma^2\left[\frac{1}{2} + \frac{1+(\varepsilon/2)}{\sigma^2}\right]}. \tag{7}$$

For $\kappa\sigma \ll 1$ the second term is negligible (except for $\varepsilon \gg 1$ or $a \ll 1$), so that $v_{x0}(\varepsilon) \approx v_0/\sqrt{1+(\varepsilon/2)}$ with $v_0 = \sqrt{0.43A\kappa\sigma}$. We verify the (range of) validity of these relations for $v_x(\varepsilon)$ and $v_{x0}(\varepsilon)$ by a numerical simulation of blob propagation for various parameters in the full-F nonlinear model Eqs. (1) and (2) using the codes TOEFL [18,20] and FELTOR [17,21]. During its propagation down the magnetic field gradient, the unstable blob develops from initially circular to a mushroom cap shape, with subsequent vortex roll-up and final turbulent breakup. Typical density structures of the rightward-propagating blob at three times ($t = 0$, 25 000, and 50 000) for $\varepsilon = 0$ (top) and $\varepsilon = 50$ (bottom) are shown in Fig. 1 for amplitude $A = 0.5$, width $\sigma = 10$ in units of ρ, and curvature $\kappa = 10^{-4}$. The computational domain is $(128\rho)^2$ with a grid resolution of 512^2. The simulation illustrates that blob transport is strongly inhibited by Debye screening.

We compare v_x with the maximum center-of-mass velocity $v_{\mathrm{sim}} \equiv \max(v_{\mathrm{com}})$ in the simulations, where $v_{\mathrm{com}} \equiv \partial_t\{\int dxdy[n_e(x,y) - n_0]x\}/\{\int dxdy[n_e(x,y) - n_0]\}$ for e-p plasmas. The maximum velocity is usually obtained in the "D-shaped" phase.

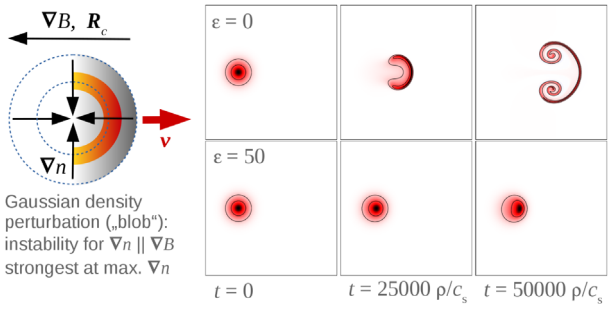

FIG. 1. Propagation of an interchange unstable electron-positron blob in quasineutral ($\varepsilon = 0$) and Debye screened plasma ($\varepsilon = 50$), shown at three times. Color scale, density n/n_0; contour lines drawn at $n/n_0 = (1.1, 1.3)$.

In Fig. 2, $v_{\mathrm{sim}}(\varepsilon)$ from the simulation (symbols) and the corresponding analytical estimates $v_x(\varepsilon)$ (continuous curves) are shown for $\kappa = 10^{-4}$ and various parameters A and σ. In all cases, the scaling $v_{x0}(\varepsilon) = v_0/\sqrt{1+(\varepsilon/2)}$ is reproduced over several orders of magnitude. The four cases shown here are $A = 0.5$ and $\sigma = 10$ [black (circles)]; $A = 0.1$ and $\sigma = 100$ [blue (stars)]; $A = 0.05$ and $\sigma = 40$ [green (diamonds)]; and $A = 0.05$ and $\sigma = 10$ [red (squares)]. Domain sizes are adapted to ensure $L_y > 10\sigma$. Quantitative agreement between the scaling law (curves) and simulations is best achieved for large amplitudes and/or small widths (i.e., the red and black cases). The largest differences appear for cases with small A and large σ (shown in blue and green), which is also found in e-i scaling laws based on energetic principles [22]. The propagation velocities drop by more than an order of magnitude for $\varepsilon > 200$.

On scales much larger than the Debye length λ, a plasma is quasineutral, and electric fields are weak. For waves or instabilities with mode numbers $k \sim \rho^{-1} \ll \lambda^{-1}$, the space charge term ($\sim\varepsilon$) in the Poisson equation (2) is negligible, as then the time for charges to adjust to quasineutrality is

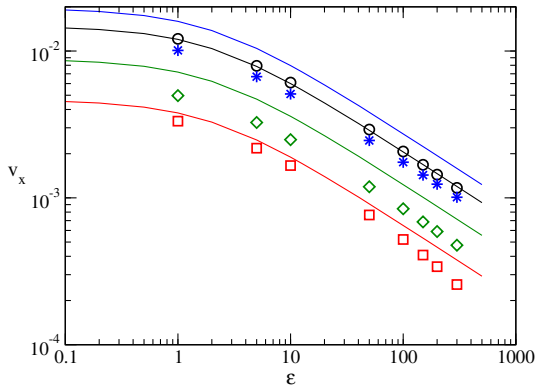

FIG. 2. Comparison of simulated (symbols) and analytical velocities (curves). Black (circles), $A = 0.5$ and $\sigma = 10$; blue (stars), 0.1 and 100; green (diamonds), 0.05 and 40; red (squares), 0.05 and 10.

much shorter than the mode evolution. For $\lambda \geq \rho$, the space charge effect in the Poisson equation is comparable to the polarization densities, which can be seen in Eq. (5): The inertial effects of polarization (given by the mass ratio term μ) and of space charging (given by ε) add up, and both reduce amplitudes for modes with large $k_\perp$. For drift scales smaller than λ, the local gradient lengths of the electric field can be of the same order as the gyration scale, and the e-p plasma oscillations ($\omega_{ep} = \sqrt{2n_e e^2/\epsilon_0 m_e}$) can occur on the same or slower time scales as the gyration time ($\omega_c = c_s/\rho$). Both have the damping effect, that energy from coherently propagating or growing drift modes can be transferred out of the present system and into local fields and e-p plasma oscillations.

In e-p plasmas, the interchange-driven density transport is consequently reduced if large values of ε can be achieved. For the projected A Positron Electron Experiment (APEX) e-p stellarator experiment [9], the major torus radius is $R = 15$ cm, and planned plasma temperatures are on the order of 0.2–2 eV at $B = 2$ T. This results in e-p gyro radii of $\rho \sim 10^{-3}$ cm. Foreseen particle densities are around 10^{13} m^{-3}, which results in Debye lengths $\lambda \sim 0.1$–0.3 cm [9]. The curvature parameter is on the order of $\kappa \sim 10^{-4}$ and $\varepsilon \sim 50$–300. An unknown quantity is the size and amplitude of emerging perturbations. For e-p plasmas, we cannot assume the same parameters for seed perturbations as in e-i plasmas, as driving drift wave vortices are absent. But as the e-p plasma is not exactly quasineutral, small local fluctuations in ϕ or N could appear spontaneously with perpendicular scales up to λ, which would correspond to $\sigma \sim 1$–200. In the Columbia Non-neutral Torus (CNT) experiment (with a field structure similar to APEX), a dominant interchange perturbation with global ($m = 1$, $n = 0$) flute mode structure was observed [23], which would correspond to $\sigma \sim 1000$. Such large perturbations could also arise in e-p plasmas, e.g., when drift waves were excited by some small fraction of ion "impurities" [24].

A complete stabilization is from Eqs. (6) and (7) obtained only for very large $\varepsilon \geq (\sigma a/\kappa) - \sigma^2$. An $\varepsilon \approx 300$, as expected in the APEX experiment [9], would not fully stabilize interchange blobs in a wide range of relevant parameters by Debye screening, but particle transport $\Gamma \sim A v_x \sim 1/\sqrt{1+(\varepsilon/2)}$ would still be reduced by around an order of magnitude. To maintain large $\varepsilon = (\lambda/\rho) = (2N_B/N_{e0})$, the e-p particle densities have to be kept at $N_{e0} \ll N_B \equiv \epsilon_0 B^2/(2m_e)$ much smaller than the Brillouin density N_B [8].

An additional background density gradient will add to the interchange driving and transport. The prediction of the level of convective transport in toroidally confined e-p plasmas has large uncertainties. As an order of magnitude estimate for APEX ($N \sim 10^{13}\,\mathrm{m}^{-3}$), we get a radial density flux $\Gamma = (AN) \times (v_x c_s) \approx (0.01 \times 10^{13}\,\mathrm{m}^{-3})(0.01 \times 10^5\,\mathrm{ms}^{-1}) \approx 10^{14}\,\mathrm{m}^{-2}\,\mathrm{s}^{-1}$.

For a plasma surface $S \sim 0.1$ m^2, this corresponds to a loss rate of 10^{13}–10^{14} s^{-1} and a confinement time of milliseconds to seconds, depending on the appearing (thermal) fluctuation levels. Our results on blob transport complement the discussion of temperature-gradient-driven instabilities in e-p plasmas in Refs. [8,11,12] but put a large uncertainty on the optimistic confinement expectations for APEX [9].

The prospect of creating macroscopic magnetically confined e-p plasmas in the laboratory motivates us to consider other possible many-body matter-antimatter systems. From symmetry principles, it appears attractive to study a system of equal numbers of electrons (e), protons (i), positrons (p), and antiprotons (a). It is unclear and, regarding present standard models of baryogenesis and magnetogenesis, highly unlikely whether such a magnetized e-i-p-a "ambiplasma" (following terminology by Alfvén) has actually ever existed in cosmic history, but it might in principle be created in a laboratory when large numbers of positrons and antiprotons could be supplied continuously at one site.

We briefly complement the above discussion by a simulation of density blobs in a quasineutral ambiplasma. The model is again given by Eqs. (1)–(3) with $s \in (e, i, p, a)$. Scales are now normalized to the proton drift scale $\rho = \sqrt{T_e m_i}/(eB)$. We initialize with a matter-antimatter symmetric density perturbation $n_s(\mathbf{x}) = n_0 + A\exp(-\mathbf{x}^2/\sigma^2)$ for all species. FLR effects are maintained for the baryons (i and a), with $\tau_i = 1$ and $\tau_a = -1$. The evolution of the ambiplasma blob by interchange driving is initially similar to e-i or e-p blobs. Remarkably, the detailed spatial matter-antimatter symmetry is twofold broken during the blob development: Fig. 3(a) shows that particle densities $N_s(x)$ deviate between species. $N_e(x)$ and $N_p(x)$ remain closely aligned and so, respectively, do $N_i(x)$ and $N_a(x)$; but leptonic and baryonic densities locally separate.

Figure 3(b) reveals that also the particle-antiparticle symmetry is locally broken, where both $(N_e - N_p)$ and $(N_i - N_a)$ differences grow with time. The curves for the e-p density difference (dashed blue curve) agree with the i-a difference (bold orange curve) through quasineutrality ($\sum_s Z_s N_s = 0$). Both are correlated with vorticity Ω.

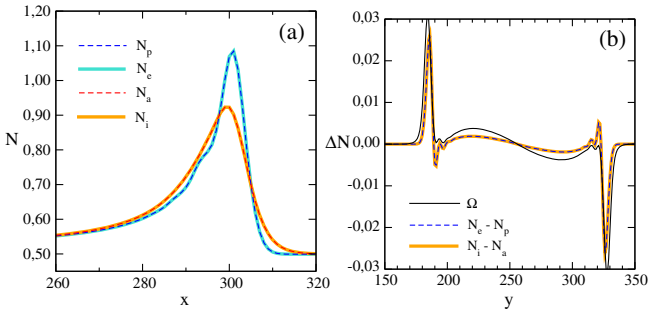

FIG. 3. Asymmetry in an ambiplasma blob: (a) Densities $N_e(x)$ and $N_p(x)$ (at y of the blob center) deviate from $N_i(x)$ and $N_a(x)$; (b) perpendicular cut through blob center: $N_e(y) - N_p(y)$ and $N_i(y) - N_a(y)$ correlate with vorticity Ω.

The local baryon-lepton asymmetry is caused by FLR effects, which mainly enter via $N_s \sim \Gamma_{1s} n_s = n_s/(1 + b_s/2)$ and reduce the densities of the massive species (baryons) in regions of steep gradients. This asymmetry disappears when FLR effects are switched off.

The breaking of the local particle-antiparticle symmetry is, in contrast, a result of interchange-driven alignment with vorticity [25] and increases with time, most pronounced at steepening blob edges. It persists when $\tau_i = \tau_a = 0$ and is thus not a FLR effect. Taking the total time derivative of the polarization equation (linearized, without FLR terms), we see that $D_t(N_p - N_e) = D_t(N_i - N_a) \sim \hat{\kappa}(N_e + N_p) \sim (\mu_i + \mu_a) D_t \Omega$. The buildup and time scale of particle-antiparticle density separation is here a consequence of vorticity generation by the interchange instability and, thus, a result of the both charge- and mass-dependent curvature or grad-B drifts and polarization under quasineutrality: The inertial baryon species drift by polarization into different regions of the (time-varying) electric field formed by the curvature drifts.

A consequence of the particle-antiparticle asymmetry appears particularly in the presence of annihilation, which is more relevant on ion drift times (compared to e-p times), and can fortify the relative particle-antiparticle density difference. A magnetized ambiplasma will lose its symmetry on combined interchange, diffusion, and annihilation time scales and in the worst case can result in patches of e-i locally separated from p-a plasma. This reduces the prospect of achieving laboratory confinement.

In summary, we have shown that the transport of plasma density by interchange driving appears for a large range of parameters in e-p plasmas. Transport is (similarly to previously discussed temperature-gradient-driven modes) significantly reduced via Debye screening for low enough densities, but derived confinement time scales bear large uncertainties. In contrast, we have further argued that sustained confinement of matter-antimatter plasmas of globally equal electron, proton, positron, and antiproton numbers is likely inhibited by local matter-antimatter separation in the presence of annihilation.

This work was supported by the Austrian Science Fund (FWF) Project No. Y398. The computational results have been achieved in part using the Vienna Scientific Cluster (VSC).

*Corresponding author.
alexander.kendl@uibk.ac.at

[1] P. A. M. Dirac, Math. Proc. Cambridge Philos. Soc. **26**, 361 (1930).
[2] ALPHA Collaboration, Nat. Phys. **7**, 558 (2011).
[3] G. Sarri *et al.*, Nat. Commun. **6**, 6747 (2015).

[4] R. Ruffini, G. Vereshchagin, and S. S. Xue, Phys. Rep. **487**, 1 (2010).
[5] J. Danielson, D. Dubin, R. Greaves, and C. Surko, Rev. Mod. Phys. **87**, 247 (2015).
[6] R. G. Greaves and C. M. Surko, Phys. Plasmas **4**, 1528 (1997).
[7] V. Tsytovich and C. B. Wharton, Comments Plasma Phys. Control. Fusion **4**, 91 (1978).
[8] T. S. Pedersen, A. H. Boozer, W. Dorland, J. P. Kremer, and R. Schmitt, J. Phys. B **36**, 1029 (2003).
[9] T. S. Pedersen, J. R. Danielson, C. Hugenschmidt, G. Marx, X. Sarasola, F. Schauer, L. Schweikhard, C. M. Surko, and E. Winkler, New J. Phys. **14**, 035010 (2012).
[10] W. Horton, Rev. Mod. Phys. **71**, 735 (1999).
[11] P. Helander, Phys. Rev. Lett. **113**, 135003 (2014).
[12] P. Helander and J. W. Connor, J. Plasma Phys. **82**, 905820301 (2016).
[13] S. I. Krasheninnikov, Phys. Lett. A **283**, 368 (2001).
[14] D. A. D'Ippolito, J. R. Myra, and S. J. Zweben, Phys. Plasmas **18**, 060501 (2011).
[15] O. E. Garcia, N. H. Bian, V. Naulin, A. H. Nielsen, and J. J. Rasmussen, Phys. Scr. **T122**, 104 (2006).
[16] J. Madsen, Phys. Plasmas **20**, 072301 (2013).
[17] M. Wiesenberger, J. Madsen, and A. Kendl, Phys. Plasmas **21**, 092301 (2014).
[18] A. Kendl, Plasma Phys. Controlled Fusion **57**, 045012 (2015).
[19] P. Helander and D. J. Ward, Phys. Rev. Lett. **90**, 135004 (2003).
[20] A. Kendl, Int. J. Mass Spectrom. **365/366**, 106 (2014).
[21] G. Danler, M.Sc. thesis, Universität Innsbruck, 2015.
[22] R. Kube, O. E. Garcia, and M. Wiesenberger, Phys. Plasmas **23**, 122302 (2016).
[23] Q. R. Marksteiner, T. Sunn Pedersen, J. W. Berkery, M. S. Hahn, J. M. Mendez, B. Durand de Gevigney, and H. Himura, Phys. Rev. Lett. **100**, 065002 (2008).
[24] H. Saleem, Q. Haque, and J. Vranjes, Phys. Rev. E **67**, 057402 (2003).
[25] A. Kendl, Phys. Plasmas **19**, 112301 (2012).